HHS Public Access

Author manuscript

Bioorg Med Chem. Author manuscript; available in PMC 2015 March 04.

Published in final edited form as:

Bioorg Med Chem. 2014 January 1; 22(1): 478–487. doi:10.1016/j.bmc.2013.11.003.

Design, Synthesis and Biological Evaluation of Ezrin Inhibitors Targeting Metastatic Osteosarcoma

Mikell Paige[a,b,*,†], **George Kosturko**[b,†], **Gullay Bulut**[c], **Matthew Miessau**[b], **Said Rahim**[c], **Jeffrey A. Toretsky**[c], **Milton L. Brown**[b], and **Aykut Üren**[c,**]

[a]George Mason University; Department of Chemistry and Biochemistry; 10900 University BLVD, MS 1A9; Manassas, VA 20110, USA

[b]Georgetown University Medical Center; Center for Drug Discovery; 3970 Reservoir Road, NW; The Research Building, Room EP07; Washington, DC 20057, USA

[c]Georgetown University Medical Center; Lombardi Comprehensive Cancer Center; 3970 Reservoir Road, NW; The Research Building, Room E316; Washington, DC 20057, USA

Abstract

Respiratory failure due to pulmonary metastasis is the major cause of death for patients with osteosarcoma. However, the molecular basis for metastasis of osteosarcoma is poorly understood. Recently, ezrin, a member of the ERM family of proteins, has been associated with osteosarcoma metastasis to the lungs. The small molecule NSC 668394 was identified to bind to ezrin, inhibit in vitro and in vivo cell migration, invasion, and metastatic colony survival. Reported herein are the design and synthesis of analogues of NSC 668394, and subsequent functional ezrin inhibition studies. The binding affinity was characterized by surface plasmon resonance technique. Cell migration and invasion activity was determined by electrical cell impedance methodology. Optimization of a series of heterocyclic-dione analogues led to the discovery of compounds **21k** and **21m** as potential novel antimetastatic agents.

1. Introduction

Although extensive research has been directed toward the prevention, detection, and treatment of cancers, high mortality due to tumor metastasis still remains a formidable challenge.[1] Osteosarcoma is a devastatingly metastatic malignancy that afflicts children and young adults, in which the majority of patients possess microscopic metastases at the time of diagnosis.[2, 3] While recent chemotherapy advancements and surgical techniques have

*CORRESPONDING AUTHOR: Mikell Paige, TEL: (703) 993-1075, FAX: (703) 993-1055, mpaige3@gmu.edu.
**CORRESPONDING AUTHOR: Aykut Üren, TEL: (202) 687-9504, au26@georgetown.edu.
†These authors have equally contributed to the paper.

6. Conflict of Interest

M.L.B., M.P., J.A.T., A.U., G.K., G.B. are co-inventors on the following patent: PCT/US2011/048635

improved the 5-year survival rate of patients with localized disease to 60–70%, patients with diagnosed metastases possess a 5-year survival rate of 30%.[3] In osteosarcoma, the main cause of death is pulmonary metastasis.[2–4] Much remains to be accomplished in developing new strategies to overcome this immense hurdle; thus, it is crucial that specific therapeutic agents be identified to target the molecular mechanisms of osteosarcoma metastasis.

Ezrin is a member of the ezrin/radixin/moesin (ERM) family of proteins that link the cell membrane to the actin cytoskeleton and are involved in pivotal cellular functions, including cell-cell adhesion, cell motility, cell shape, cell proliferation and apoptosis.[5–9] ERM proteins are composed of three distinct regions: 1) an amino-terminal membrane-binding domain, 2) an α-helical midsection, and 3) a carboxyl-terminal actin-binding domain.[5–9] Ezrin exhibits no intrinsic enzymatic activity and exerts its biological functions through protein-protein interactions generated upon its conformational change. Quiescent ezrin adopts an intramolecular head-to-tail amino-carboxyl termini complex, which can be modified by specific molecular interactions. Two factors are involved in this conformational transition: binding of the amino-terminal domain to phosphatidylinositol 4,5-biphosphate and phosphorylation of a conserved threonine 567 (T567) in the actin-binding domain.[5–9] The resulting conformation perturbation creates new molecular interactions with both the plasma membrane and cortical cytoskeleton including adhesion molecules such as CD43, CD44, ICAM-1 and ICAM-2 either directly or through adapter proteins.[8, 9]

Of late, high ezrin expression has been identified as vital for metastatic behavior in a murine osteosarcoma model and its over-expression has been linked to a poor prognosis in murine, canine, and human OS cases.[10, 11] Furthermore, elevated levels of ezrin have translated to poor clinical outcomes in other metastatic malignancies including rhabdomyosarcoma and pancreatic cancer.[12–14] We have recently identified that a small molecule, NSC 668394, is a potent inhibitor of ezrin function as determined by inhibiting migration in both in vitro and in vivo models. Moreover, inhibition of threonine 567 phosphorylation by NSC 668394 significantly reduced the metastatic behavior in cellular and animal models and has thus emerged as an important lead inhibitor. [15]

Consequently, we conducted a series of systematic structure-activity relationship (SAR) studies with NSC 668394 independently targeting various chemical moieties of the molecular framework (Figure 1). Herein, we identify novel scaffolds that maintain drug-like properties yet possess improved functional activity for targeting the dynamic phases of ezrin-dependent metastasis.

2. Experimental Section

All reagents and solvents were purchased from commercial suppliers and used as received unless noted otherwise. Flash column chromatography separations were done on a Biotage SP1 system monitoring at 254 and 310 nm. NMR spectra were recorded on a Varian 400MR spectrometer at 22.5 °C, operating at 400 MHz for ^{1}H and 100 MHz for ^{13}C NMR. The chemical shifts are expressed in ppm downfield from TMS as an internal standard ($CDCl_3$ or DMSO-d_6 solution). Microwave chemistry was performed in sealed reaction vessels in a CEM Discover instrument operating at 150W. The temperature for microwave experiments

was monitored using a built-in infrared detection system, and the reactions were run at the specified temperature and time as stated in the experimental details.

Isoquinoline-5,8-dione (3).[16]

A solution of 0.51 g (3.5 mmol) of 5-hydroxyisoquinoline (**2**) in 50 mL of acetonitrile was cooled to 0 °C under a nitrogen atmosphere. To 100 mL of a 2:1 acetonitrile-water solution was dissolved 3.2 g (7.6 mmol) of (bis trifluoroacetoxy) iodobenzene (PIFA). The PIFA solution was added dropwise to the pre-cooled solution of 5-hydroxyisoquinoline over a 30-min time period. The reaction solvent was concentrated under reduced pressure to afford a dark brown aqueous solution. The aqueous solution was extracted with ethyl acetate (3 × 100 mL). The organic extract was washed with brine (50 mL), dried over magnesium sulfate, filtered, and concentrated under reduced pressure to give a dark yellow residue. The residue was purified by silica gel column chromatography eluting with 1:4 ethyl acetate-hexanes to give 0.19 g, (34%) of isoquinoline-5,8-dione as bright yellow crystals. ^{1}H NMR (400 MHz, $CDCl_3$) δ: 9.15 (d, J = 1.5 Hz, 1 H), 9.07 (dd, J = 1.5, 8.1 Hz, 1 H), 7.82 (d, J = 8.1 Hz, 1 H), 7.04 (d, J = 10.4 Hz, 1 H), 6.91 (d, J = 10.4 Hz, 1 H). ^{13}C NMR (100.17 MHz, $CDCl_3$) δ: 182.1, 181.0 149.7, 148.5, 140.3, 138.1, 137.8, 130.9, 120.2.

Phthalazine-5,8-dione (5).[17, 18]

A solution of 3.0 g (23.3 mmol) of phthalazine in 20 mL of concentrated sulfuric acid was brought to 100 °C. To the phthalazine solution was added portion-wise 18.8 g (186 mmol) of potassium nitrate over 1-h time period. After 72 h at 100 °C, the solution was cooled to room temperature, poured over ice, and neutralized with ammonium hydroxide to produce a yellow-tan precipitate. The precipitate was collected and dried to afford 2.3 g (56%) of the 5-nitrophthalazine intermediate as a light yellow solid. ^{1}H NMR (400 MHz, DMSO-d_6) δ: 10.2 (s, 1 H), 9.98 (s, 1 H), 8.84 (d, J = 7.4 Hz, 1 H), 8.59 (d, J = 7.6 Hz, 1 H), 8.20 (dd, J = 7.4, 14.9 Hz, 1 H). ^{13}C NMR (100.17 MHz, DMSO-d_6) δ: 152.1, 146.3, 141.0, 133.2, 131.8, 130.0, 127.4, 118.7.

To 0.88 g (5.0 mmol) of 5-nitrophthalazine in 30 mL of tetrahydrofuran at 50 °C was added 4.37 g (25.1 mmol) of sodium hydrogen sulfite in 15 mL of water. The reaction mixture was stirred at 50 °C for 15 min. The organic solution was extracted with ethyl acetate (3 × 100 mL), washed with brine (50 mL), and dried over magnesium sulfate. Filtration and removal of the solvent under reduced pressure gave the product as a bright yellow precipitate. The precipitate was recrystallized in a hot methanol solution to afford 0.49 g (67%) of 5-aminophthalazine. ^{1}H NMR (400 MHz, DMSO-d_6) δ: 9.80 (s, 1 H), 9.60 (s, 1 H), 7.60 (dd, J = 4. 6, 7.6 Hz, 1 H), 7.20 (dd, J = 1.9, 4.6 Hz, 1 H), 7.02 (d, J = 7.6 Hz, 1 H), 6.50 (s, 2 H). ^{13}C NMR (100.17 MHz, DMSO-d_6) δ: 150.1, 146.5, 145.1, 133.2, 126.1, 114.7, 114.1, 112.2.

To 0.40 g (2.75 mmol) of 5-aminophthalazine in 25 mL of 10% sulfuric acid solution at 0 °C was added 1.11 g (3.73 mmol) of sodium dichromate. After 30 min, the solution was extracted with dichloromethane (3 × 100 mL). The organic extract was dried with magnesium sulfate, filtered, and concentrated under reduced pressure to afford 0.064 g (28%) of the desired phthalazine-5,8-dione as a red solid. ^{1}H NMR (400 MHz, DMSO-d_6) δ:

9.80 (s, 1 H), 7.20 (s, 1 H). 13C NMR (100.17 MHz, DMSO-d_6) δ: 184.5, 146.2, 139.3, 124.2.

Quinoline-5,8-dione (7).[19]

To a solution of 1.5 g (7.9 mmol) of 5-nitro-8-hydroxyquinoline in 100 mL of anhydrous tetrahydrofuran under a nitrogen atmosphere at 55 °C was added dropwise 6.89 g (39.6 mmol) of sodium hydrogen sulfite in 60 mL of water. After a 15-min reaction time, the solution was cooled to room temperature and extracted with ethyl acetate (3 × 150 mL). The isolated organic extract was washed with brine, dried over magnesium sulfate, filtered, and concentrated under reduced pressure to give a yellow solid. The solid was purified by silica gel column chromatography eluting with 3:2 ethyl acetate-hexanes to afford 0.80 g (63%) of 5-amino-8-hydroxyquinoline as bright yellow crystals. ^{1}H NMR (400 MHz, $CDCl_3$) δ: 8.89 (d, J = 4.8 Hz, 1 H), 8.71 (s, 1 H), 8.41 (d, J = 8.6 Hz, 1 H), 7.74 (dd, J = 4.8, 8.6 Hz, 1 H), 6.89 (d, J = 7.5 Hz, 1 H), 6.65 (d, J = 7.5 Hz, 1 H), 5.25 (s, 2 H). ^{13}C NMR (100.17 MHz, $CDCl_3$) δ: 149.9, 143.9, 138.0, 137.3, 130.7, 122.6, 120.8, 116.1, 112.5.

To 0.80 g (5.0 mmol) of 5-amino-8-hydroxyquinoline in 150 mL of CH_2Cl_2 at 0 °C was added 150 mL of a 5% aqueous solution of H_2SO_4 followed by slow addition of a pre-cooled solution of 2.98 g (10.0 mmol) of sodium dichromate in 50 mL of H_2O at 0 °C. The yellow solution became orange and biphasic. After 1 h, the reaction was extracted with methylene chloride and washed with brine. The organic extract was dried over magnesium sulfate and filtered. The solvent was removed under reduced pressure to give a yellow solid. The solid was purified using silica gel column chromatography eluting 3:2 ethyl acetate-hexanes to afford 0.49 g (61%) of quinoline-5,8-dione. ^{1}H NMR (400 MHz, $CDCl_3$) δ: 8.90 (d, J = 4.6 Hz, 1 H), 8.71 (s, 1 H), 8.41 (d, J = 8.1 Hz, 1 H), 7.74 (dd, J = 4.6, 8.1 Hz, 1 H), 7.06 (d, J = 10.9 Hz, 1 H), 6.90 (d, J = 10.9 Hz, 1 H). ^{13}C NMR (100.17 MHz, $CDCl_3$) δ: 182.1, 180.7, 148.8, 147.2, 138.2, 138.1, 135.4, 129.0, 128.3.

General reaction conditions for synthesis of compounds 18, 19, 20, NSC 668394, and 21a through 21m—To a solution of the substituted tyramine (1.2 equiv) in ethanol (~30 mM solution) is added heterocyclic dione structure (1.0 equiv) and DIEA (1.2 equiv.) at room temperature under a nitrogen atmosphere. The reaction vessel is refluxed for 5 h and then concentrated under reduced pressure. The residue is purified by silica gel column chromatography eluting with methylene chloride as methanol as the mobile phase.

2-((3,5-dibromo-4-hydroxyphenethyl)amino)naphthalene-1,4-dione (18): Yield: 0.056 g (0.13 mmol, 20% yield)—^{1}H NMR (400 MHz, DMSO-d_6) δ: 9.78 (s, 1 H), 7.95 (m, 2 H), 7.80 (dd, J = 1.5, 7.5 Hz, 1 H), 7.75 (dd, J = 1.5, 7.5 Hz, 2 H), 7.51 (s, 2 H), 5.81 (s, 1 H), 3.41 (m, 2 H), 2.91 (t, J = 7.3 Hz, 2 H). ^{13}C NMR (100.17 MHz, DMSO-d_6) δ: 182.1, 181.8, 148.9, 148.1, 134.7, 133.4, 133.0, 132.4, 132.0, 130.2, 125.8, 125.2, 111.7, 99.7, 42.8, 31.5.

7-((3,5-dibromo-4-hydroxyphenethyl)amino)isoquinoline-5,8-dione (19): Yield: 0.028 g (0.13 mmol, 20% yield)—^{1}H NMR (400 MHz, DMSO-d_6) δ: 9.15 (d, J = 1.9 Hz, 1 H), 9.07 (dd, J = 1.9, 8.1 Hz, 1 H), 7.82 (d, J = 8.1 Hz, 1 H), 7.61 (s, 1 H), 7.41 (s, 2

H), 5.92 (s, 1 H), 3.44 (m, 2 H), 2.87 (t, *J* = 7.3, 2 H). ^{13}C NMR (100.17 MHz, DMSO-d_6) δ: 181.7, 180.9, 150.4, 149.2, 148.5, 145.1, 140.3, 139.9, 133.6, 133.1, 130.1, 112.2, 100.6, 41.3, 31.4.

6-((3,5-dibromo-4-hydroxyphenethyl)amino)phthalazine-5,8-dione (20a): Yield: 0.072 g (0.13 mmol, 20% yield)—^{1}H NMR (400 MHz, DMSO-d_6) δ: 9.71 (s, 1 H), 9.60 (s, 1 H), 7.91 (s, 1 H), 7.45 (s, 2 H), 5.95 (s, 1 H), 3.47 (m, 2 H), 2.84 (t, *J* = 7.1 Hz, 2 H). ^{13}C NMR (100.17 MHz, DMSO-d_6) δ: 181.7, 180.9, 150.4, 149.2, 148.5, 145.1, 140.3, 139.9, 133.6, 133.1, 130.1, 112.2, 100.6, 41.3, 31.4.

7-(phenethylamino)quinoline-5,8-dione (21a): Yield: 0.048 g (0.17 mmol, 79%) —^{1}H NMR (400 MHz, DMSO-d_6) δ: 9.01 (d, *J* = 4.6 Hz, 1 H), 8.32 (d, *J* = 8.0 Hz, 1 H), 7.72 (dd, *J* = 4.6, 8.0 Hz, 1 H), 7.60 (t, *J* = 6.1 Hz, 1 H), 7.40 (dd, *J* = 4.1, 8.2 Hz, 1 H), 7.29 (d, *J* = 8.1 Hz, 1 H), 7.27 (dd, *J* = 1.8, 4.2 Hz, 1 H), 5.90 (s, 1 H), 3.34 (q, *J* = 6.7 Hz, 2 H), 2.81 (t, *J* = 7.3 Hz, 2 H). ^{13}C NMR (100.17 MHz, DMSO-d_6) δ: 181.5, 180.0, 154.5, 149.2, 148.5, 147.8, 133.8, 133.5, 127.4, 127.1,126.4, 111.8, 101.1, 42.9, 31.6.

7-((3-chlorophenethyl)amino)quinoline-5,8-dione (21b): Yield: 0.013 g (0.041 mmol, 11%)—^{1}H NMR (400 MHz, DMSO-d_6) δ: 8.95(d, *J* = 4.5 Hz, 1 H), 8.31 (d, *J* = 7.9 Hz, 1 H), 7.74 (dd, *J* = 4.5, 7.9 Hz, 1 H), 7.60 (t, *J* = 6.0, 1 H), 7.49 (d, *J* = 8.1 Hz, 1 H), 7.34 (dd, *J* = 4.2, 8.0 Hz, 1 H), 7.31 (d, *J* = 4.2 Hz, 1 H), 7.17 (d, *J* = 1.9 Hz, 1 H), 5.91 (s, 1 H), 3.26 (q, *J* = 6.5 Hz, 2 H), 2.82 (t, *J* = 7.1 Hz, 2 H). ^{13}C NMR (100.17 MHz, DMSO-d_6) δ: 181.5, 180.0, 154.5, 148.5, 147.8, 140.9, 134.2, 133.8, 133.7, 130.0, 129.1, 127.3, 126.0, 125.9, 101.3, 42.8, 31.7.

7-((3-bromophenethyl)amino)quinoline-5,8-dione (21c): Yield: 0.031 g (0.087 mmol, 24%)—^{1}H NMR (400 MHz, DMSO-d_6) δ: 8.97 (d, *J* = 4.7 Hz, 1 H), 8.34 (d, *J* = 8.0 Hz, 1 H), 7.76 (dd, *J* = 4.8, 8.0 Hz, 1 H), 7.49 (d, *J* = 7.9 Hz, 1 H), 7.34 (dd, *J* = 1.9, 7.9 Hz, 1 H), 7.31 (d, *J* = 4.1 Hz, 1 H), 7.17 (d, *J* = 4.1 Hz, 1 H), 5.94 (s, 1 H), 5.82 (s, 1 H), 3.42 (q, *J* = 6.6, 2 H), 2.82 (t, *J* = 7.1, 2 H). ^{13}C NMR (100.17 MHz, DMSO-d_6) δ: 182.3, 181.4, 155.1, 149.2, 148.3, 141.1, 135.2, 132.7, 130.1, 129.4, 128.7, 128.1, 126.7, 121.0, 101.3, 42.8, 31.7.

7-((3-chloro-4-methoxyphenethyl)amino)quinoline-5,8-dione (21d): Yield: 0.015 g (0.087 mmol, 10%)—^{1}H NMR (400 MHz, $CDCl_3$) δ: 9.01 (d, 1 H), 8.34 (d, 1 H), 7.55 (m, 1 H), 7.60 (m, 1 H), 7.21 (m, 1 H), 7.05 (m, 1 H), 6.90 (m, 1 H), 5.96 (s, 1 H), 5.91(s, 1 H), 3.89 (s, 3 H), 3.45 (m, 2 H), 2.90 (m, 2 H). ^{13}C NMR (100.17 MHz, $CDCl_3$) δ: 181.4, 181.2, 155.1, 154.0, 149.2, 147.2, 134.7, 130.5, 130.2, 127.7, 127.3 126.2, 122.8, 112.4, 102.2, 56.2, 43.6, 33.1.

7-((3-bromo-4-methoxyphenethyl)amino)quinoline-5,8-dione (21e): Yield: 0.036 g (0.093 mmol, 15%)—^{1}H NMR (400 MHz, $CDCl_3$) δ: 9.00 (d, 1 H), 8.31 (d, 1 H), 7.57 (m, 1 H), 7.58 (m, 1 H), 7.47 (m, 1 H), 7.06 (m, 1 H), 6.92 (m, 1 H), 5.95 (s, 1 H), 5.90 (s, 1 H), 3.84 (s, 3 H), 3.41 (m, 2 H), 2.87 (m, 2 H). ^{13}C NMR (100.17 MHz, $CDCl_3$) δ: 181.6, 180.5, 155.5, 153.8, 149.0, 147.1, 134.9, 130.7, 130.0, 127.5, 127.1 126.5, 122.4, 112.2, 102.4, 56.4, 43.1, 32.7.

7-((3,4-dihydroxyphenethyl)amino)quinoline-5,8-dione (21g): Yield: 0.018 g (0.055 mmol, 10%)—^{1}H NMR (400 MHz, DMSO-d_6) δ: 8.97 (d, 1 H), 8.71 (s, 1 H), 8.34 (d, 1 H), 7.63 (m, 1 H), 7.42 (s, 1 H), 6.86 (d, 1 H), 6.73 (m, 2 H), 5.92 (s, 1 H), 3.35 (m, 2 H), 2.78 (m, 2 H). ^{13}C NMR (100.17 MHz, DMSO-d_6) δ: 181.8, 180.4, 155.7, 150.4, 148.2, 145.9, 145.1, 136.3, 134.7, 132.0, 130.3, 123.7, 116.2, 115.5, 100.7, 41.1, 31.6.

7-((3,4,5-trihydroxyphenethyl)amino)quinoline-5,8-dione (21h)—^{1}H NMR (400 MHz, DMSO-d_6) δ: 8.94 (d, 1 H), 8.32 (d, 1 H), 7.61 (m, 1 H), 7.51 (s, 1 H), 6.42 (s, 2 H), 5.92 (s, 1 H), 3.41 (m, 2 H), 2.84 (m, 2 H). ^{13}C NMR (100.17 MHz, DMSO-d_6) δ: 181.3, 180.2, 154.1, 149.2, 148.1, 147.3, 136.2, 133.1, 132.5, 127.4, 126.4, 109.8, 100.3, 41.7, 32.0.

7-((3,4-dimethoxyphenethyl)amino)quinoline-5,8-dione (21i): Yield: 0.014 g (0.043 mmol, 12%)—^{1}H NMR (400 MHz, $CDCl_3$) δ: 8.91 (d, 1 H), 8.40 (d, 1 H), 7.61 (m, 1 H), 6.83 (m, 3 H), 6.03 (s, 1 H), 5.91 (s, 1 H), 3.81 (s, 3 H), 3.79 (s, 3 H), 3.40 (m, 2 H), 2.92 (m, 2 H). ^{13}C NMR (100.17 MHz, $CDCl_3$) δ: 181.4, 180.3, 153.2, 149.3, 148.1, 146.7, 140.0, 134.1, 132.0, 130.8, 130.0, 128.3, 120.7 111.7, 111.6, 100.4, 56.0, 59.4, 44.0, 33.9.

7-((3,4-bis(benzyloxy)phenethyl)amino)quinoline-5,8-dione (21j): Yield: 0.079 g (0.24 mmol, 39%)—^{1}H NMR (400 MHz, $CDCl_3$) δ: 9.01 (d, 1 H), 8.18 (d, 1 H), 7.60 (m, 1 H), 7.58–7.20 (m, 10 H), 6.81–6.74 (m, 3 H), 5.91 (s, 1 H), 5.08 (d, 4 H), 3.41 (m, 2 H), 2.91 (m, 2 H). ^{13}C NMR (100.17 MHz, $CDCl_3$) δ: 181.9, 180.4, 154.9, 149.1, 148.8, 148.3, 147.3, 137.9, 137.8, 134.3, 132.4, 128.8, 128.7, 128.2, 128.1, 128.0, 127.9, 127.8, 126.9, 121.8, 115.7, 115.2, 101.3, 70.7, 70.6, 43.8, 33.4.

7-((3,5-dichloro-4-hydroxyphenethyl)amino)quinoline-5,8-dione (21k): Yield: 0.13 g (0.41 mmol, 57%)—^{1}H NMR (400 MHz, DMSO-d_6) δ: 8.92 (d, 1 H), 8.32 (d, 1 H), 7.61 (m, 1 H), 7.51 (s, 1 H), 7.28 (s, 2 H), 5.91 (s, 1 H), 3.39 (m, 2 H), 2.81 (m, 2 H). ^{13}C NMR (100.17 MHz, DMSO-d_6) δ: 181.5, 180.0, 154.5, 149.0, 148.7, 147.9, 133.9, 133.5, 132.5, 127.4, 126.4, 111.8, 101.9, 42.9, 31.6.

7-((3,5-difluoro-4-hydroxyphenethyl)amino)quinoline-5,8-dione (21l): Yield: 0.063 g (0.189 mmol, 30%)—^{1}H NMR (400 MHz, DMSO-d_6) δ: 9.91 (s, 1 H), 8.97 (d, J = 4.3 Hz, 1 H), 8.27 (d, J = 8.0 Hz, 1 H), 7.71 (dd, J = 4.3, 8.0 Hz, 1 H), 7.51 (s, 1 H), 7.01 (d, J = 9.4 Hz, 2 H), 5.89 (s, 1 H), 3.41 (q, J = 6.6 Hz, 2 H), 2.81 (t, J = 7.2 Hz, 1 H). ^{13}C NMR (100.17 MHz, DMSO-d_6) δ: 182.1, 180.3, 155.1, 153.9, 150.8, 149.2, 148.7, 134.1, 130.2 (d, J = 11.1 Hz, C-F coupling), 128.0, 127.2, 112.1, 100.3, 43.1, 32.3.

7-((4-hydroxy-3,5-dimethylphenethyl)amino)quinoline-5,8-dione (21m): Yield: 0.058 g (0.18 mmol, 18%)—^{1}H NMR (400 MHz, DMSO-d_6) δ: 8.91 (d, J = 4.6 Hz, 1 H), 8.25 (d, J = 8.1 Hz, 1 H), 8.0 (s, 2 H), 7.80 (dd, J = 4.6, 8.0 Hz, 1 H), 7.60 (s, 1 H), 5.91 (s, 1 H), 3.38 (m, 2 H), 2.79 (t, J = 7.1 Hz, 2 H), 2.03 (s, 6 H). ^{13}C NMR (100.17 MHz, DMSO-d_6) δ: 180.5, 178.1, 154.1, 150.6, 147.4, 147.0, 132.0, 127.2, 126.8, 124.5, 123.8, 122.1, 99.7, 41.1, 30.1, 15.1.

6-(3,5-dibromo-4-hydroxyphenethyl)-5*H*-pyrrolo[3,4-*b*]pyridine-5,7(6*H*)-dione (22a):[20, 21]**—**To a solution of 1.33 g (3.52 mmol) of compound **10** in 1.0 mL of DMF in a microwave tube, was added 0.50 g (3.35 mmol) of compound **8** and 0.36 g (0.35 mmol) of triethylamine. The microwave tube was sealed and heated in a microwave at 150 °C for 4 h. After 4 h, the reaction mixture was added to water and the tan colored product precipitated from the solution. The precipitate was taken up in methylene chloride and impregnated onto silica gel. Purification by silica gel column chromatography eluting with 5% methanol in methylene chloride afforded 0.87 g (58%) of compound **22a** as an off-white solid.

^{1}H NMR (400 MHz, DMSO-d_6) δ: 8.88 (d, J = 4.6 Hz, 1 H), 8.09 (d, J = 8.0 Hz, 1 H), 7.40 (dd, J = 4.6, 8.0 Hz, 1 H), 7.31 (s, 2 H), 6.56 (s, 1 H), 3.67 (q, J = 6.7 Hz, 2 H), 2.84 (t, J = 7.2 Hz, 2 H). ^{13}C NMR (100.17 MHz, DMSO-d_6) δ: 168.2, 167.4, 152.6, 148.1, 146.2, 135.3, 135.0, 132.1, 128.9, 120.0, 111.7, 42.8, 31.5.

Evaluation of small molecule binding to recombinant ezrin was performed by Surface Plasmon Resonance Spectroscopy as follows:

A Biacore CM5 sensorchip was initially primed three times with HBS-P (0.01 M HEPES pH 7.4, 0.15 M NaCl, 0.005% v/v Surfactant P20) buffer, followed by EDCI and *N*-hydroxysuccinimide solutions (720 sec). Recombinant ezrin protein was loaded onto the CM5 chip in a pH 5.5 acetate buffer at a rate of 10μL/min for capturing ~12,000 RU, followed by a 720 sec ethanolamine block cycle. A running buffer containing (10% DMSO, 25 mM Tris pH 7.5, 10 mM $MgCl_2$, 0.5 mM EGTA, 0.5 mM Na_3VO_4, 5 mM β-glycerophosphate, 0.01% Triton X-100, 200 mM ATP) was used for the binding analysis of inhibitors to recombinant ezrin. As a positive control, compound NSC 668394 was injected at 25 μM to recombinant ezrin and allowed to interact with the protein for 60 seconds, and washed off the protein with the running buffer for 500 seconds. The protein surface was then regenerated in a 1:500 solution of H_3PO_4.

After the initial binding studies, the small molecules that bound to the recombinant ezrin protein were further evaluated to identify their binding affinity. The methodology for the binding kinetics experiment is as follows. As a positive control, compound NSC 668394 was injected at 1.56, 3.125, 6.25, 12.5 and 25.0 μM concentrations to calculate the binding kinetics of the reaction. Each hit molecule from the different structure classes were evaluated independently with NSC 668394 and injected at the concentrations listed above. Mean binding steady state affinities (K_D) and standard deviations were calculated from three independent experiments for each compound.

Chemotaxis/Cell Migration assay

Cell migration experiments were performed using the Roche Xcelligence electric cell impedance instrument, which allowed for ‘real-time’ and label free analysis of cell migration. Each CIM 16 well migration plate contained an 8 μm permeable membrane between the top and bottom chamber. The bottom chamber was solvated with 160 μL of 10% fetal bovine serum media containing 1% DMSO as the chemoattractant, with serum free media as a negative chemoattractant control. Next, the top chamber was solvated with 150 μL of a premixed cell solution. Each cell solution was composed of 1.5×10^5 K7M2 or

K12 cells in serum free media containing 1% DMSO, along with the small molecule. Total concentration of the small molecule in the cell solution was 2 μM. The cell solution without any small molecule was used as the positive control. Cell migration was monitored in 'real-time' for 24 hours and percent migratory inhibition was determined by the migration ratio of the small molecule, divided by the migration of the positive control.

3. Results

To investigate if the inhibitory properties of NSC 668394 were restricted to the quinoline-5,8-dione framework, we synthesized positional isomers of the quinone substructure. Though the carbocyclic naphthylquinone **1** was readily available, a series of corresponding heterocyclic-dione analogues were synthesized. As shown in Scheme 1, PIFA hypervalent iodide oxidation of 8-isoquinolinol (**2**) provided isoquinoline-5,8-dione (**3)**. However, synthesis of the phthalazine-dione substructure required a more formidable methodology.[16] Selective nitration of commercially available phthalazine (**4**) in the presence of KNO_3 afforded 5-nitrophthalazine in a 61% yield. Sodium dithionite reduction and subsequent chromium oxidation smoothly afforded phthalazine-5,8-dione (**5)**, albeit in moderate yield.[22, 23] Similar chemical methodologies were employed to convert the available 5-nitro-8-hydroxyquinoline (**6)** to the quinoline-5,8-dione scaffold **7**. Following sodium dithionite reduction, direct conversion of 5-amino-8-hydroxyquinoline to **7** was effected with the use of potassium dichromate under acidic conditions.[24] Additional heterocyclic scaffolds that lacked the α,β-unsaturated dione system but contained the dicarbonyl moiety were envisioned as potential ring constricted analogues, with 2,3-dipyridinedicarboxylic anhydride (**8**) as the ideal platform for this structure class.

Though SAR investigation of the aromatic side-chain was expedited by the commercial availability of functionalized β-phenethylamines, the desired 3,5-disubstituted tyramine scaffolds required a more involved synthetic route. As shown in Scheme 2, the 3,5-dibromotyramine·HBr salt **10** was synthesized from the unprotected tyramine **9**. The 3,5-dichlorotyramine·HCl salt **11** was synthesized by chlorination of N-acyltyramine with sulfuryl chloride.[25] Subsequent acidic-mediated deprotection afforded the desired salt.[26] The 3,5-difluorotyramine·HCl salt **16** and 3,5-dimethyl tyramine·HCl salt **17** were generated from the functionalized nitrostyrene intermediates **14** and **15**, respectively. Condensation of the appropriate benzaldehydes **12** and **13** under Henry reaction conditions provided compounds **14** and **15**, respectively, which were further modified to the requisite amines via reduction with lithium aluminum hydride.[27] Following isolation, the corresponding β-phenethylamine scaffold **16** and **17** were acidified with HCl to afford their corresponding HCl salts. [28]

As outlined in Scheme 3, treatment of the synthesized heterocyclic-dione fragments with the susbtituted β-phenethylamine afforded the desired functionalized ring architectures **18**-**22** by Michael-addition to the α,β-unsaturated core. Analogue **22a** was synthesized by microwave-assisted condensation of the anhydride scaffold **8**. Reactions with the isoquinoline-dione **3** and quinoline-dione **7** frameworks resulted in a mixture of regioisomers for analogues **19** and **21**, which were separated by silica gel column chromatography.[29]

With the development of this series of analogues we took advantage of the opportunity to systematically investigate the structure activity relationship. We evaluated the effects of these chemical modifications on binding to recombinant ezrin protein by surface-plasmon resonance spectroscopy. OS cell migration and HUVEC monolayer invasion was determined in 'real-time' by electrical impedance technologies. Additional functional assays to validate the lead candidates included inhibition of ezrin phosphorylation and disruption of protein-protein interactions.

First, we evaluated the library of compounds based on their potential for a direct interaction between the analogues and recombinant ezrin protein. Analysis of ezrin binding potency was accomplished using a surface plasmon resonance assay, which measured the direct binding of the synthetic inhibitor delivered by a microfluidic system to the immobilized recombinant ezrin protein.[15] Real-time kinetic data for the small molecules binding the recombinant protein, including k_{on} and k_{off} rates were determined based on a 1:1 binding model.

As shown in Table 1, the positional substitution pattern on the heterocyclic framework impacted compound affinity to recombinant ezrin. While the heterocyclic compound NSC 668394 has a binding affinity K_D of 10.6 ± 2.9 μM to recombinant ezrin, the direct binding could not be determined for its carbocyclic analogue **18a** due to aggregation. Modification to the isoquinoline-5,8-dione analogue **19a** resulted in a 4-fold decrease in binding from the quinoline-5,8-dione congener, while substitution to the di-aza phthalazine-5,8-dione analogue **20a** could not be determined due to aggregation. Substitution of the α,β-unsaturated dione system of NSC 668394 to the ring-constricted pyridino-phthalimide derivative **22a**, resulted in a complete loss of ezrin binding potency.

Upon determining that the quinoline-dione framework possessed the highest affinity to recombinant ezrin, we subsequently evaluated the various quinoline-dione analogues with functionalized aromatic side chains to investigate ezrin binding with positional isomers of NSC 668394. As shown in Table 2, the substitution pattern on the β-phenethylamine scaffold also perturbed affinity of the analogues for binding to recombinant ezrin. The NSC 668394 binding affinity (K_D = 10.6± 2.9μM) in comparison to analogue **21a**, which showed no binding to ezrin, suggested that the 3,5 dibromo-4-hydroxy substitution pattern on the aryl ring is important for ezrin binding. Addition of hydroxyl substituents on the aromatic group as shown for analogues **21f**[21] and **21g** resulted in slightly increased binding affinity to ezrin. Substitution of the bromine atoms with chlorine atoms as shown in analogue **21k** also resulted in a statistically significant increase in ezrin-binding potency. Substitution of the chlorine atoms in analogue **21k** with fluorine atoms (**21l**) led to a 5-fold decrease in binding. We further investigated the effect of replacing the bromine substituents with CH_3 groups. To our surprise, the dimethyl analogue **21m** also afforded a statistically significant increase in ezrin binding affinity over NSC 668394.

It was hypothesized that in the cell, the quinone core could intercalate double-stranded DNA and result in non-specific cytotoxicity. We modified a reported fluorescent DNA intercalation assay designed by Cain and coworkers to examine the intercalation activity of the designed ezrin inhibitors on double-stranded DNA.[30] As shown in Figure 2, titration of a Hoechst 33258:double-stranded DNA complex with compound NSC 668394 resulted in

minimal inhibition of DNA fluorescence while titration with doxorubicin, a known DNA intercalating chemotherapeutic, resulted in a significant reduction in complex fluorescence. We confirmed that despite a similar quinone framework between the two molecules, NSC 668394 does not intercalate double-stranded DNA.

In light of the binding studies, we employed a series of secondary screening methods to confirm the small molecule interaction with cellular ezrin in biochemical assays. In order to evaluate critical ezrin cellular function, cell viability limits were identified for each compound prior to investigating their ability to inhibit ezrin function. We chose the highly metastatic murine cell line K7M2, expressing high levels of ezrin protein and its congener K12 cell line, expressing low levels of ezrin.[10, 11] K7M2 and K12 cell viability was measured with compounds **18a**-**22a**. The viable concentrations and IC_{50} values were identified. (See Supplemental Tables 1 and 2). Since loss of ezrin does not affect cell viability or survival of K7M2 and K12 cells, concentrations giving cell death were considered non-specific toxicity beyond ezrin inhibition. Blocking ezrin function is expected to inhibit cell motility and invasion at the cellular level. Therefore, all experiments were done at a dose and time range of compounds that do not kill the cells.

Metastasis is a complex multi-step process in which the disease spreads to distal sites through the blood system. Specific phenotypes including migration, invasion and extravasion are pivotal for survival at the satellite location.[31, 32] Both the migration and invasion phenotype and their inhibition can be studied in-vitro using real-time electrical impedance-based technology. The ROCHE RTCA CIM-16 plate is a Boyden chamber that detects the migration of cells through an 8 μm membrane coated with electronic sensors. This method can accurately monitor the migration of metastatic cells in ‘real-time’ and label free. Inhibition of K7M2 and K12 cell migration was investigated at a non-toxic concentration of 2 μM for compounds **18a**-**22a** over 24 hours. The degree of inhibition of K7M2 and K12 cell migration are presented in Figure 3. Similar to the plasmon resonance analysis in Tables 1 and 2, the functional groups on the aryl side-chain and heterocyclic substructure proved to be important for activity. The quinoline-dione substructure as shown in NSC 668394 was found to play an important role in selectivity for inhibition of ezrin-dependent migration when compared to analogues **18a**, **19a**, **20a** and **22a**, which contain different heterocyclic systems. To our surprise, both analogues **21f** and **21g**, which contain the tyramine or dopamine scaffolds, respectively, lacked ezrin-specific migratory inhibition activity despite their potent binding affinity to recombinant ezrin. Additionally, this ezrin-specificity was enhanced when the bromine atoms of NSC 668394 were substituted for chlorine groups as shown for analogue **21k**. However, further chemical transformation to either the difluoro or dimethyl substituents as shown for analogues **21l** and **21m**, respectively, resulted in a decrease activity in cell migration. The decreased activity of **21m** was unexpected in light of its potent binding kinetics as determined by SPR. We can only speculate that the lack of correlation for this compound may be due to the need to disrupt protein-protein interactions, which suggests that simply binding to ezrin does not necessarily result in disrupting the function of the protein.

Chemotaxis inhibition is just one component in targeting cellular metastatic potential as motile cells may still possess the capability for endothelial layer invasion to a colonized

location.[33, 34] Moreover, tumor cell-endothelial cell interaction can be duplicated in vitro using electrical-impedance technology. We recently optimized an invasion assay that monitored the disruption of a monolayer of human umbilical vein endothelial cells (HUVEC) with invasive tumor cells.[35] The invasion potential of the tumor cell is measured by the changes in cell impedance as the HUVEC monolayer junctions is compromised by the invading tumor cell.

Initially, we identified analogues that had a minimum 2-fold inhibition threshold of K7M2/K12 cell migration and selected those for HUVEC invasion analysis. We considered compounds below the 2-fold threshold as non-specific for ezrin inhibition. Next, we identified a 9-hour timeline in which the invading tumor cell completely disrupted the HUVEC monolayer junctions, which we forecasted would require a higher concentration (10 μM) of the ezrin inhibitor for the invasion study. Following the HUVEC toxicity screening at the escalated concentration, we monitored the anti-invasion activity of the candidate inhibitors on both the high ezrin expressed K7M2 and low ezrin expressed K12 osteosarcoma cells as outlined in Figure 4. A trend observed in both the binding kinetics and chemotaxis assays were consistent in the invasion assay. From Figure 4, it is important to note that our lead inhibitor NSC 668394 has a 2.39 fold difference in the ratio of K7M2/K12 invasion inhibition, while other heterocyclic systems, such as the isoquinoline-dione scaffold **19a**, phthalazine-dione scaffold **20a**, or the ring-condensed pyridinyl-phthalimide substructure **22a** lacked any selectivity (1.20-, 1.07-, and 0.32-fold ratio, respectively) (See Figure 4). Of note, analogues **21d**, **21k** and **21m** resulted in similar binding kinetics to that of NSC 668394, and were effective at inhibiting ezrin-mediated HUVEC monolayer invasion with an inhibition ratio of 2.67, 3.01 and 3.93, respectively (See Figure 4). Therefore, we selected analogues **21d**, **21k**, and **21m** as suitable lead candidates, since each resulted in notable ezrin binding potency and enhanced anti-migration and invasion activity as compared to NSC 668394. These compounds were selected for additional biochemical evaluation to assess the effect of these analogues on ezrin with regards to metastatic inhibition.

The functional activity of ezrin is believed to be due to an intrinsic enzymatic activity but from conformational changes upon threonine 567 (T567) phosphorylation.[36,37] Phosphorylation of T567 leads to a conformational change in its tertiary structure, by reducing the affinity of the C-terminal domain for the N-terminal domain.[8] This structural perturbation yields an open conformation that allows proteins, such as F-actin to bind to ezrin. The site-specific modification of T567 with alanine (T567A) was shown to prevent ezrin phosphorylation.[11] Moreover, Khanna and coworkers have shown that this T567A modification results in complete inhibition of experimental metastases in a murine OS model. We investigated if the lead analogues **21d**, **21k**, **21m,** and **21a** abrogate metastatic phenotypes by inhibiting critical T567 phosphorylation by ezrin immunoprecipitation experiments. K7M2 cells were treated with analogues **21d**, **21k 21m,** or **22a** for 6 h at 10 μM and subjected to immunoprecipitation with an ezrin antibody, followed by immunoblotting with a T567 phospho-ezrin, actin and ezrin antibodies. As shown in Figure 5, both analogues **21k** and **21m** resulted in a reduced T567 phosphorylation expression as compared to NSC 668394 without modifying the overall total expression of ezrin.

4. Discussion

For the past two decades, our knowledge of the genetic and epigenetic events involved in the early events of tumorigenesis has increased considerably. By contrast, despite the appreciation of the clinical relevance of tumor metastasis, there is a lack of therapies that can effectively target this phenotype. The identification of NSC 668394 has yielded the first “targeted therapy” approach for metastatic osteosarcoma by investigating ezrin, a cytoskeletal protein linking membrane-bound proteins with cytosolic scaffolding proteins. Our intention was to synthesize analogues of NSC 668394 with enhanced potency and optimized functional activity for targeting the malignant stages of metastasis. We explored the importance of the heterocyclic-dione substructure and the structural requirements of the substituted β-phenethylamine side-chain.

Four different and largely independent assay systems were used to characterize the analogues. The assays were designed to determine specificity for targeting ezrin in the developmental stages of metastasis. Our initial analysis of ezrin specificity was performed using surface plasmon resonance spectroscopy to determine the affinity and binding kinetics of our inhibitors to recombinant ezrin protein. Our secondary chemotaxis assay mirrored the early stages of sarcoma metastasis, which involves tumor cell migration through the circulatory system. Our study afforded compounds that were specific for ezrin inhibition and subsequently chemotaxis. Proximal stages of sarcoma metastasis rely on tumor cell invasion through endothelial layers for colony survival. We further evaluated this progression using electrical impedance-based technology and identified novel scaffolds that have both ezrin specific anti-migration activities in addition to anti-invasion potentials, which exceed the results determined for our lead compound NSC 668394.

An unexpected outcome of this study was that the binding kinetics of analogues as **21d, 21g**, **21k**, and **21m** did not result in substantial improvement over the lead candidate NSC 668394. This may reflect the nature of binding to an intrinsically disordered protein, where a single “best fit” between the compound and the target may in fact not exist. Thus, the protein conformation that optimally interacts with the quinoline-dione substructure and the aromatic side chain may be quite different from that of the isoquinoline-dione, phthalazine-dione, or phthalimide core. Binding a particular protein conformation consequently yields an entropic penalty either from organization of certain residues into a binding conformation or from selecting one particular structure out of the array of possible conformations. The current optimized molecules may not be able to capture a sufficiently large region of the ezrin protein in an energetically favorable way such that structural modifications can afford cumulative increases in binding affinities.

Despite the above caveats, our results do indicate that simple alterations of the index compound NSC 668394 can lead to significant improvements in targeting the ezrin function. On the basis of our results, these analogues selectively target ezrin and have the potential for affecting metastasis.

Supplementary Material

Refer to Web version on PubMed Central for supplementary material.

Acknowledgments

Support for our work came from the Children's Cancer Foundation of Baltimore, US Department of Defense (W81XWH-10-1-0137), Brandon Carrington Lee Pediatric Cancer Foundation, Dani's Foundation and Cancer Center Support Grant P30 CA051008 for use of Biacore Molecular Interaction Shared Resource. We would like to thank to Ms. Veronica Rodriguez for excellent technical support.

References

1. Perez L, Danishefsky SJ. Chemistry and biology in search of antimetastatic agents. ACS Chem Biol. 2007; 2:159–62. [PubMed: 17373763]
2. Meyers PA, Gorlick R. Osteosarcoma. Pediatr Clin North Am. 1997; 44:973–89. [PubMed: 9286295]
3. Meyers PA, Heller G, Healey JH, Huvos A, Applewhite A, Sun M, LaQuaglia M. Osteogenic sarcoma with clinically detectable metastasis at initial presentation. J Clin Oncol. 1993; 11:449–53. [PubMed: 8445419]
4. Marina N, Gebhardt M, Teot L, Gorlick R. Biology and therapeutic advances for pediatric osteosarcoma. Oncologist. 2004; 9:422–41. [PubMed: 15266096]
5. Tsukita S, Yonemura S. ERM (ezrin/radixin/moesin) family: from cytoskeleton to signal transduction. Curr Opin Cell Biol. 1997; 9:70–5. [PubMed: 9013673]
6. Tsukita S, Oishi K, Sato N, Sagara J, Kawai A. ERM family members as molecular linkers between the cell surface glycoprotein CD44 and actin-based cytoskeletons. J Cell Biol. 1994; 126:391–401. [PubMed: 7518464]
7. Smith WJ, Nassar N, Bretscher A, Cerione RA, Karplus PA. Structure of the active N-terminal domain of Ezrin. Conformational and mobility changes identify keystone interactions. J Biol Chem. 2003; 278:4949–56. [PubMed: 12429733]
8. Carvalho K, Khalifat N, Maniti O, Nicolas C, Arold S, Picart C, Ramos L. Phosphatidylinositol 4,5-bisphosphate-induced conformational change of ezrin and formation of ezrin oligomers. Biochemistry. 2010; 49:9318–27. [PubMed: 20873751]
9. Heiska L, Alfthan K, Gronholm M, Vilja P, Vaheri A, Carpen O. Association of ezrin with intercellular adhesion molecule-1 and -2 (ICAM-1 and ICAM-2). Regulation by phosphatidylinositol 4, 5-bisphosphate. J Biol Chem. 1998; 273:21893–900. [PubMed: 9705328]
10. Khanna C, Khan J, Nguyen P, Prehn J, Caylor J, Yeung C, Trepel J, Meltzer P, Helman L. Metastasis-associated differences in gene expression in a murine model of osteosarcoma. Cancer Res. 2001; 61:3750–9. [PubMed: 11325848]
11. Khanna C, Wan X, Bose S, Cassaday R, Olomu O, Mendoza A, Yeung C, Gorlick R, Hewitt SM, Helman LJ. The membrane-cytoskeleton linker ezrin is necessary for osteosarcoma metastasis. Nat Med. 2004; 10:182–6. [PubMed: 14704791]
12. Yu Y, Khan J, Khanna C, Helman L, Meltzer PS, Merlino G. Expression profiling identifies the cytoskeletal organizer ezrin and the developmental homeoprotein Six-1 as key metastatic regulators. Nat Med. 2004; 10:175–81. [PubMed: 14704789]
13. Akisawa N, Nishimori I, Iwamura T, Onishi S, Hollingsworth MA. High levels of ezrin expressed by human pancreatic adenocarcinoma cell lines with high metastatic potential. Biochem Biophys Res Commun. 1999; 258:395–400. [PubMed: 10329398]
14. Yeh TS, Tseng JH, Liu NJ, Chen TC, Jan YY, Chen MF. Significance of cellular distribution of ezrin in pancreatic cystic neoplasms and ductal adenocarcinoma. Arch Surg. 2005; 140:1184–90. [PubMed: 16365240]
15. Bulut G, Hong SH, Chen K, Beauchamp EM, Rahim S, Kosturko GW, Glasgow E, Dakshanamurthy S, Lee HS, Daar I, Toretsky JA, Khanna C, Uren A. Small molecule inhibitors of

ezrin inhibit the invasive phenotype of osteosarcoma cells. Oncogene. 2012; 31:269–81. [PubMed: 21706056]

16. Barret R, Daudon M. Oxidation of phenols to quinones by bis(trifluoroacetoxy)iodobenzene. Tetrahedron Letters. 1990; 31:4871–4872.
17. Gomtsyan A, Bayburt EK, Schmidt RG, Zheng GZ, Perner RJ, Didomenico S, Koenig JR, Turner S, Jinkerson T, Drizin I, Hannick SM, Macri BS, McDonald HA, Honore P, Wismer CT, Marsh KC, Wetter J, Stewart KD, Oie T, Jarvis MF, Surowy CS, Faltynek CR, Lee CH. Novel transient receptor potential vanilloid 1 receptor antagonists for the treatment of pain: structure-activity relationships for ureas with quinoline, isoquinoline, quinazoline, phthalazine, quinoxaline, and cinnoline moieties. J Med Chem. 2005; 48:744–52. [PubMed: 15689158]
18. Ryu CK, Park RE, Ma MY, Nho JH. Synthesis and antifungal activity of 6-arylamino-phthalazine-5,8-diones and 6,7-bis(arylthio)-phthalazine-5,8-diones. Bioorg Med Chem Lett. 2007; 17:2577–80. [PubMed: 17320386]
19. Farnsworth, ALNCO.; Han, HCAZ.; Vankayalapati, HSLCUT.; Warner, SLTAZ.; Von Hoff, DDSAZ.; Bearss, DHUT. Protein tyrosine phosphatase-prl-1 a a marker and therapeutic target for pancreatic cancer. US. 2007/0026398 A1. 2007.
20. Murakata M, Yamada K, Hoshino O. Studies on synthesis of araplysillins via oxidative cyclisation of o-phenolic oxime-acid derivatives using phenyliodonium diacetate. Heterocycles. 1998; 47:921–931.
21. Wada Y, Harayama Y, Kamimura D, Yoshida M, Shibata T, Fujiwara K, Morimoto K, Fujioka H, Kita Y. The synthetic and biological studies of discorhabdins and related compounds. Org Biomol Chem. 2011; 9:4959–76. [PubMed: 21597627]
22. Shaikh IA, Johnson F, Grollman AP. Streptonigrin. 1. Structure-activity relationships among simple bicyclic analogues. Rate dependence of DNA degradation on quinone reduction potential. J Med Chem. 1986; 29:1329–40. [PubMed: 3525839]
23. Parrick J, Ragunathan R. Studies of phthalazine-5,8-quinone, A ring contraction, and some novel and potentially useful fluorescent phthalimides. Journal of the Chemical Society, Perkin Transactions. 1993; 1:211–216.
24. Boger DL, Duff SR, Panek JS, Yasuda M. Inverse electron demand Diels-Alder reactions of heterocyclic azadienes. Studies on the total synthesis of lavendamycin: investigative studies on the preparation of the CDE .beta. -carboline ring system and AB quinoline-5,8-quinone ring system. J Org Chem. 1985; 50:5782–5789.
25. Diers JA, Pennaka HK, Peng J, Bowling JJ, Duke SO, Hamann MT. Structural activity relationship studies of zebra mussel antifouling and antimicrobial agents from verongid sponges. J Nat Prod. 2004; 67:2117–20. [PubMed: 15620267]
26. Schoenfeld RC, Conova S, Rittschof D, Ganem B. Cytotoxic, antifouling bromotyramines: a synthetic study on simple marine natural products and Their analogues. Bioorg Med Chem Lett. 2002; 12:823–5. [PubMed: 11859011]
27. Blanco-Pillado, M-JIIN.; Chappell, MDNIN.; De La Torre, MGM.; Diaz Buezo, NM.; Fritz, JEMIN.; Holloway, WGZIN.; Matt, JEFIN.; Mitch, CECIN.; Pedregal-Tercero, CM.; Wuimby, SJNIN.; Siegel, MGIIN.; Smith, DRWIN.; Stucky, RDIIN.; Takeuchi, KIIN.; Thomas, EMCIN.; Wolfe, CNNIN. Diaryl ethers as opioid receptor antagonist. US. 2006/0217372 A1. 2006.
28. Kita Y, Takada T, Ibaraki M, Gyoten M, Mihara S, Fujita S, Tohma H. An Intramolecular Cyclization of Phenol Derivatives Bearing Aminoquinones Using a Hypervalent Iodine Reagent. J Org Chem. 1996; 61:223–227.
29. Hargreaves RH, David CL, Whitesell LJ, Labarbera DV, Jamil A, Chapuis JC, Skibo EB. Discovery of quinolinediones exhibiting a heat shock response and angiogenesis inhibition. J Med Chem. 2008; 51:2492–501. [PubMed: 18363347]
30. Cain BF, Baguley BC, Denny WA. Potenial antitumor agents. 28. Deoxyribonucleic acid polyintercalating agents. J Med Chem. 1978; 21:658–68. [PubMed: 671464]
31. Klein CA. Cancer. The metastasis cascade. Science. 2008; 321:1785–7. [PubMed: 18818347]
32. Chiang AC, Massague J. Molecular basis of metastasis. N Engl J Med. 2008; 359:2814–23. [PubMed: 19109576]

33. Orr FW, Wang HH, Lafrenie RM, Scherbarth S, Nance DM. Interactions between cancer cells and the endothelium in metastasis. J Pathol. 2000; 190:310–29. [PubMed: 10685065]

34. Christofori G. New signals from the invasive front. Nature. 2006; 441:444–50. [PubMed: 16724056]

35. Rahim S, Uren A. A real-time electrical impedance based technique to measure invasion of endothelial cell monolayer by cancer cells. J Vis Exp. 2011

36. Ren L, Hong SH, Cassavaugh J, Osborne T, Chou AJ, Kim SY, Gorlick R, Hewitt SM, Khanna C. The actin-cytoskeleton linker protein ezrin is regulated during osteosarcoma metastasis by PKC. Oncogene. 2009; 28:792–802. [PubMed: 19060919]

37. Matsui T, Yonemura S, Tsukita S. Activation of ERM proteins in vivo by Rho involves phosphatidyl-inositol 4-phosphate 5-kinase and not ROCK kinases. Curr Biol. 1999; 9:1259–62. [PubMed: 10556088]

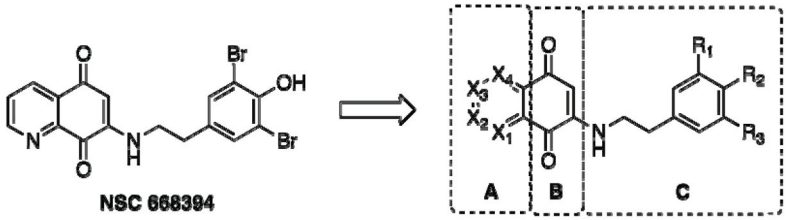

Figure 1.
Structure-Activity-Relationship of NSC 668394

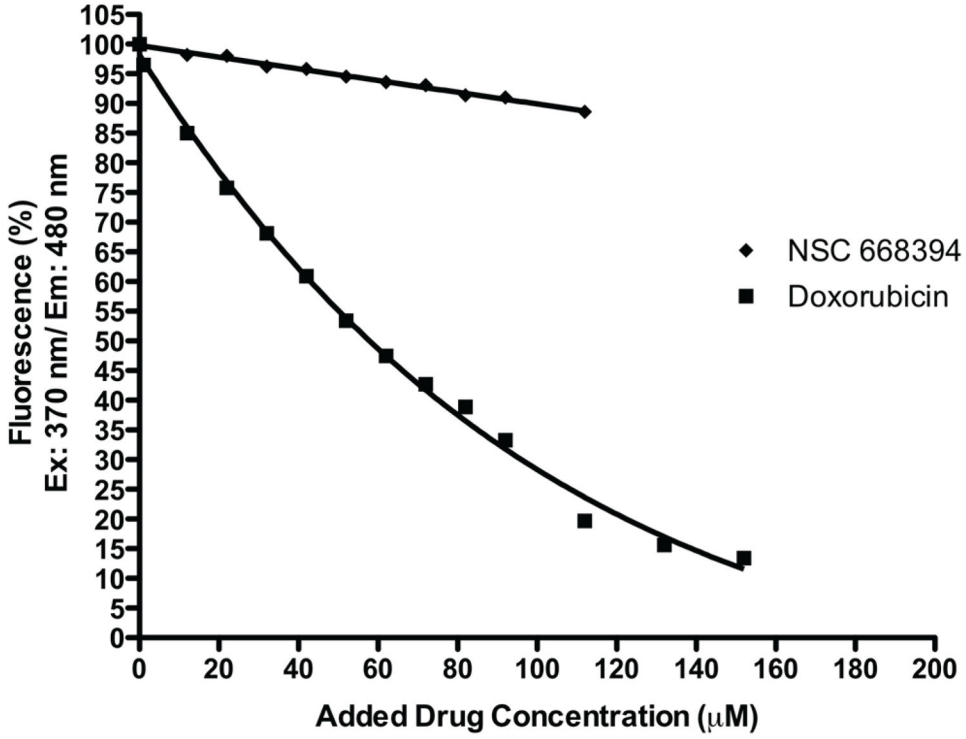

Figure 2. DNA Intercalation studies with doxorubicin and NSC 668394

Decrease in Hoescht 33258-DNA fluorescence following addition of doxorubicin [■] or NSC 668394 [◆]. Excitation at 370 nm and emission at 480 nm in a 0.01 SHE buffered solution. Initial Hoescht 33258 and Type 1 calf thymus DNA concentrations were 5 μM And 100 μL of 1.0 mg/mL, respectively. Fluorescence values are provided as percentages of the maximum.

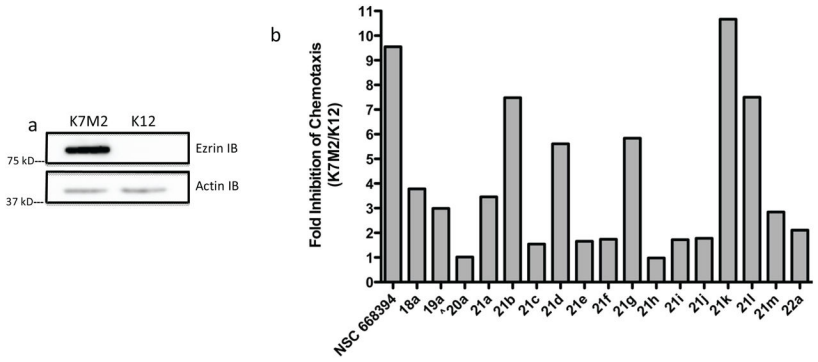

Figure 3. Inhibition of Osteosarcoma cell motility

(**a**) Immunoblotting showed that the K7M2 cell line had higher levels of ezrin protein expression than K12 cells. (**b**) Small molecule-mediated inhibition of metastatic cell migration. Transwell migration assay where K7M2 and K12 cells were treated for 24 h with small molecule at 2 μ M concentrations unless noted. ^ K7M2 and K12 cells were treated with small molecule at 1 μ M concentrations for 24 h.

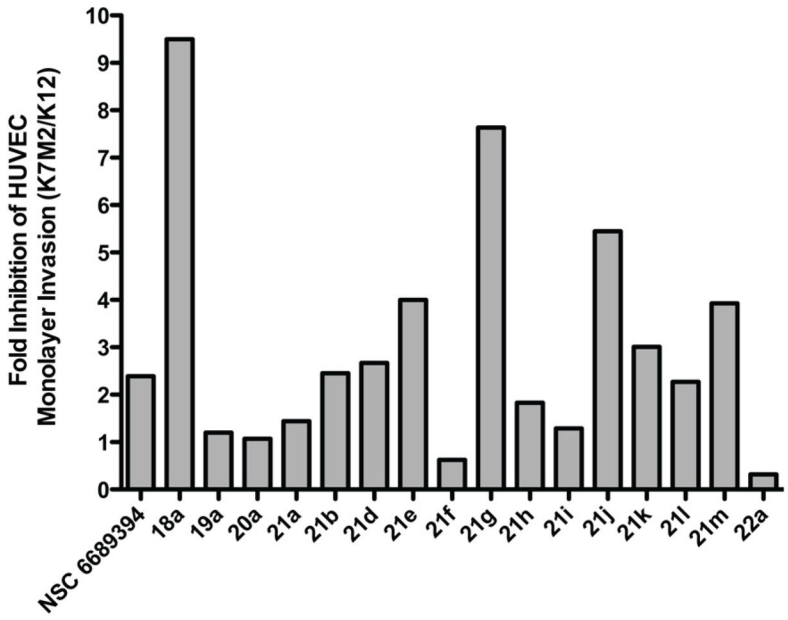

Figure 4. Inhibition of Osteosarcoma cell invasion on HUVEC monolayer

A confluent monolayer of HUVEC cells was challenged with K7M2 or K12 murine metastatic osteosarcoma cells and the anti-invasion activity of the ezrin inhibitor was validated using electrical cell impedance technology. Experiments were Performed in duplicated and the invading OS cells were treated with or without the presence of 10 μ M of ezrin inhibitors. Invasion was quantified at 9h post addition of osteosarcoma cells and results are expressed as a fold inhibition of K7M2 and K12 cell invasion.

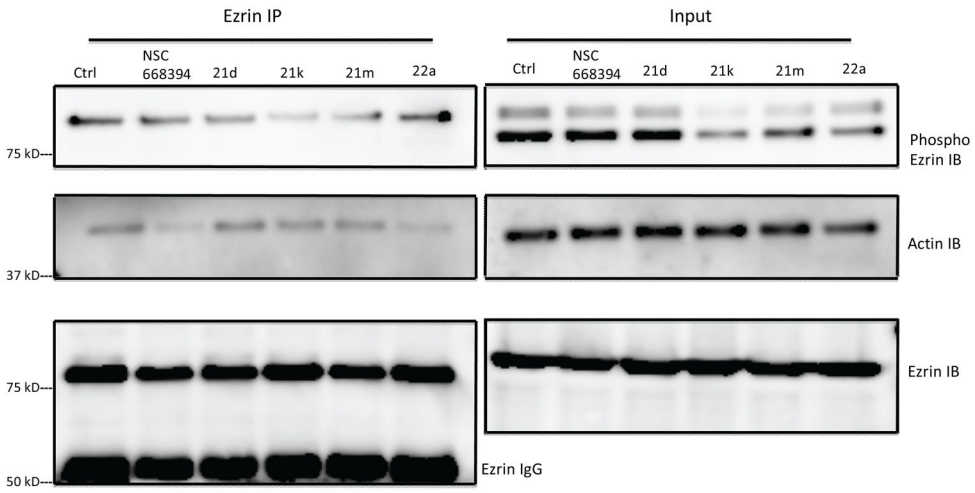

Figure 5. Small molecules inhibit Ezrin T567 phosphorylation

Compounds inhibit phosphorylation of endogeneous ezrin protein and interaction with actin without altering cellular ezrin levels. K7M2 cells were treated with NSC668394, 21d, 21k, 21m and 22a (10 μM) for 6h and subjected to immunoprecipitation with ezrin antibody followed by Immunoblotting with phospho-ezrin, actin and ezrin antibodies. Control lane is DMSO (1%) K7M2 lysate.

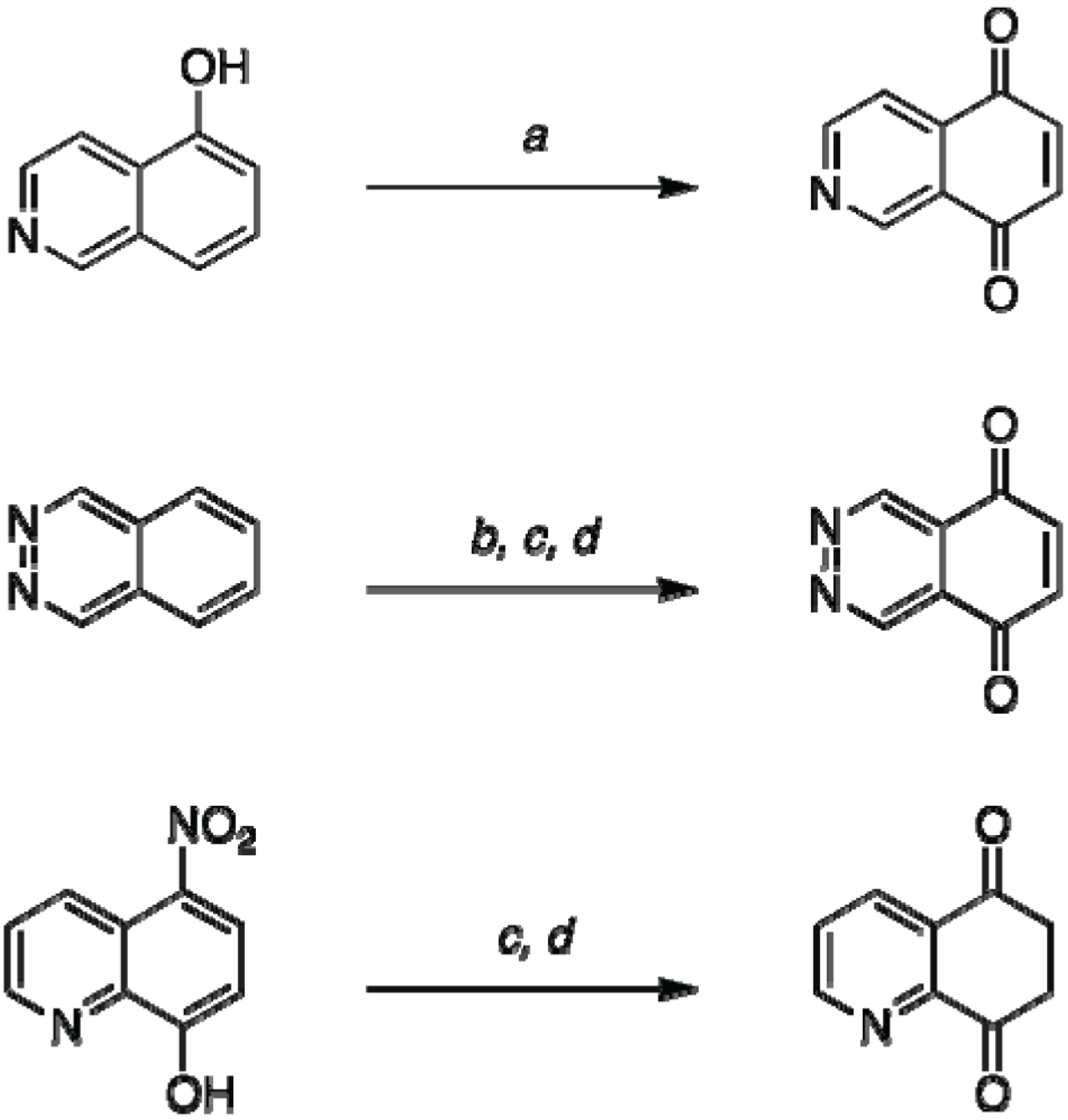

Scheme 1. Synthesis of Heterocyclic-dione substructures

(a) Ph-I($OCOCF_3$)$_2$, H_2O-CH_3CN, 0 °C, 2 h (41%); *(b)* KNO_3, H_2SO_4, 100 °C, 72 h (61%); *(c)* $Na_2S_2O_4$, THF, reflux, 0.5 h (52%); *(d)* $Na_2Cr_2O_7$, 5% H_2SO_4, H_2O, 0 °C, 0.5 h (67%).

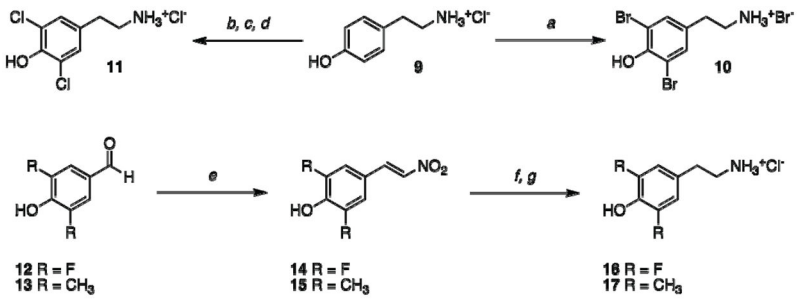

Scheme 2. Synthesis of substituted β-phenethylamine side-chain

(a) Br_2, MeOH, reflux, 12 h (91%); *(b)* Ac_2O, $NaHCO_3$, THF-H_2O, 4 h, rt (87%); *(c)* SO_2Cl_2, Et_2O, rt, 12 h (47%); *(d)* HCl, AcOH, reflux, 14 h (83%); *(e)* CH_3NO_2, NH_4OAc, AcOH, 2 h, reflux (55–71%); *(f)* $LiAlH_4$, $AlCl_3$, THF, 0 °C-rt, 16 h; *(g)* HCl, n-BuOH-$PhCH_3$ (72–78%).

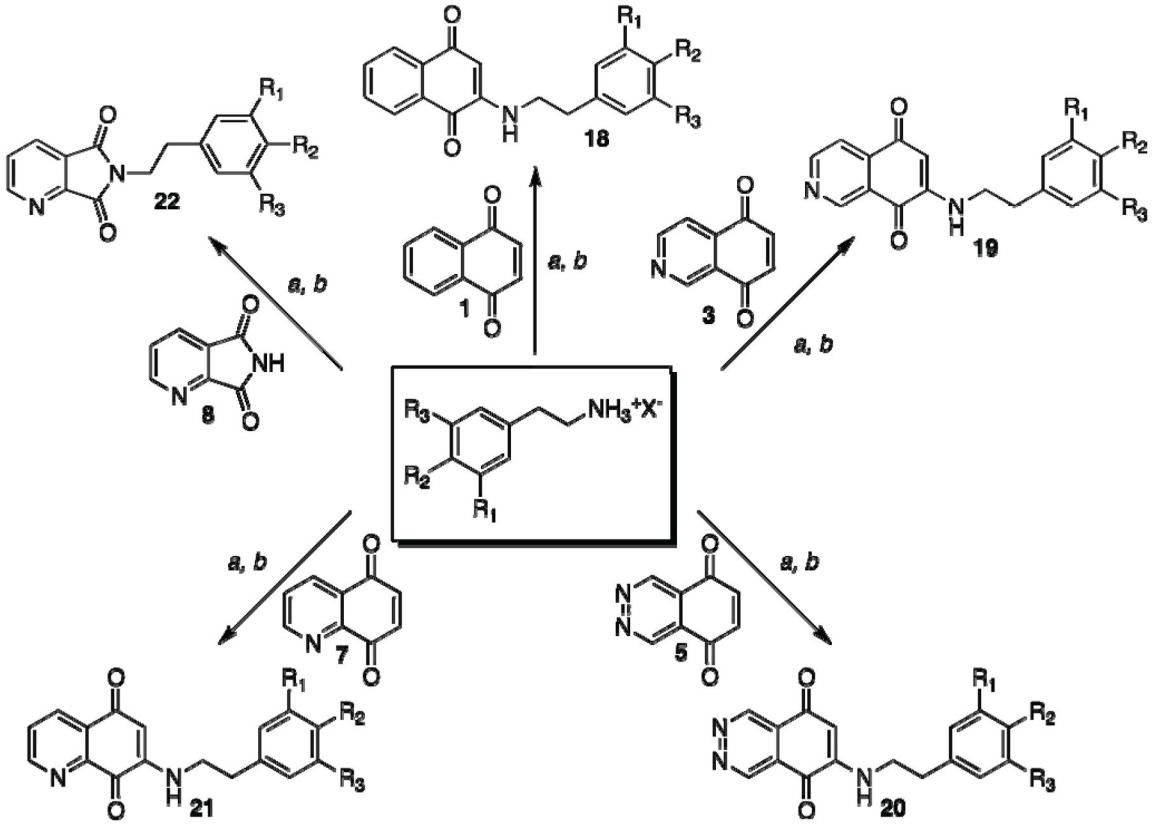

Scheme 3. SAR synthesis of NSC 668394 analogs

(a) EtOH, Et3N, reflux, 5 h *(b)* air oxidation (31–68%); *(c)* AcOH, DIEA, microwave, 140 °C, 2 h (81–89%).

Bioorg Med Chem. Author manuscript; available in PMC 2015 March 04.

Table 1

Binding Affinities of Analogs to Recombinant Ezrin: Heterocyclic-diones

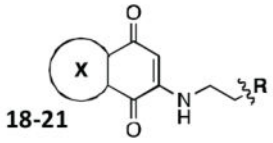

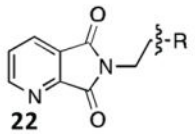

ID	NSC668394	18a	19a	20a	22a
R	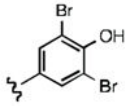	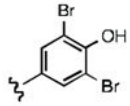	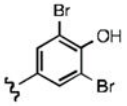	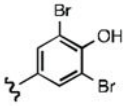	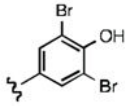
X					-
^{a} K_D (μ M)	10.6 ±2.9	Agg	40.1 ±16.3	Agg	NB^{b}
K_{on} ($M^{-1}s^{-1}$)	289.24±92.08	-	84.9 ±1.4	-	-
K_{off} (s^{-1})	0.00293 ± 0.0005	-	0.00328 ± 0.00133	-	-
cLogP	3.96	5.01	3.96	3.05	3.40

^{a}Binding affinities determined by surface plasmon resonance spectrometry (BIACORE). Kinetics experiments were run in triplicate unless noted. In each kinetics experiment, compound was injected in triplicate at 7 different concentrations, ranging from 0 to 50 μ M. Mean KD values and standard deviations were calculated from three independent experiments for each compound.

^{b}NB= no binding.

^{c}Agg= aggregate formed during binding study.

Table 2

Binding Affinities of Analogs to Recombinant Ezrin: Quinoline-diones

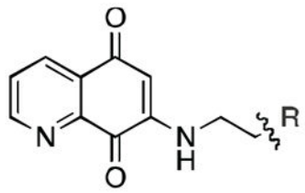

ID	NSC 668394	21a	21b	21c	21d	21e	21f	21g	21h	21i	21j	21k	21l	21m
R	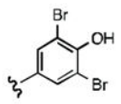	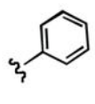	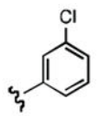	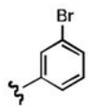	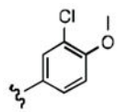	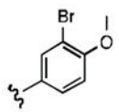	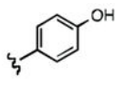	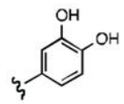	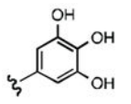	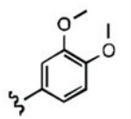	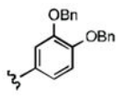	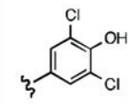	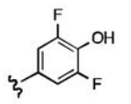	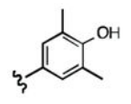
a K_D(μM)	10.6±2.9	NB*b*	NB*b*	9.1	7.0 ±3.4	27.4 *F*	6.9 ±1.9	7.9 ±1.8	Agg*c*	NB*b*	25.3 *F*	8.0 ±2.2	49.9±12.2	5.0 ±0.6
P value		–	–	–	0.072	-	0.034	0.016	-	-	-	0.013	-	0.003
K_{on} ($M^{-1}s^{-1}$)	289.24±92.08	-	-	609.9 ± 137.7	286.9±92.8	-	1151.0±342.7	754.7 ± 210.4	-	-	-	525.4 ± 54.65	19.4 ± 4.7	706.8 ± 157.7
K_{off} (s^{-1})	0.00293 ± 0.0005	-	-	0.00146±0.007	0.0041±0.00035	-	0.0036±0.0007	0.00555±0.0009	-	-	-	0.00338 ± 0.00147	0.00163 ± 0.0003	0.00355 ± 0.00121
cLogP	3.92	3.062	3.78	3.93	3.60	3.75	2.40	1.80	1.13	2.72	6.26	3.56	2.68	3.29

*a*Binding affinities determined by surface plasmon resonance spectrometry. Kinetics experiments were run in triplicate unless noted. In each kinetics experiment, compound was injected in triplicate at 7 different concentrations, ranging from 0 to 50 μM. Binding data was correlated to a 1:1 binding mode and mean KD values and standard deviations were calculated from three independent experiments for each compound.

*F*Binding data was correlated to a steady-state affinity binding model.

*b*NB= no binding.

*c*Agg= aggregate formed during binding study.